EPTT-2024-XXXX
NUMERICAL STUDY OF A TOROIDAL PROPELLER

Vinicius do Vale
University of Blumenau (FURB) – Blumenau – SC
vvale@furb.br

Higor de Bitencourt Rodrigues
Federal University of Santa Catarina (UFSC) – Florianópolis – SC
higordebitencourt@gmail.com

Alícia Carvalho Ribeiro
Federal University of Santa Catarina (UFSC) – Florianópolis – SC
aliciar@furb.br

Guilherme do Nascimento
Regional University of Blumenau (FURB), Blumenau, SC, Brazil
gdnascimento@furb.br

Jonathan Utzig
University of Blumenau (FURB) – Blumenau – SC
jutzig@furb.br

Abstract. *The applications of UAVs (Unmanned Air Vehicles) are expanding in various industries, particularly in defense and agriculture. As an emerging technology, numerous studies have been conducted to examine different aspects of UAVs. This study aims to investigate the effects of different propeller geometries on UAV performance, with a focus on comparing a conventional propeller and a toroidal propeller. For the analysis of the toroidal propeller, Computational Fluid Dynamics (CFD) serves as a valuable tool to predict flow behavior, pressure, and flow rate. Significant effort has been made to predict flow behavior efficiency, primarily using the Reynolds-averaged Navier-Stokes (RANS) approach, which several studies have identified as the most effective method. To achieve this objective, numerical simulations will be performed using the Multi Reference Frame (MRF) method to simulate the motion forces generated by the propeller in the airflow. Initial results indicate that the optimal meshing approach involves a total of 1,750,320 cells.*

Keywords: *Computational Fluid Dynamics, toroidal propeller, turbulent kinetic energy, Reynolds-averaged Navier-Stokes*

1. INTRODUCTION

Unmanned Aerial Vehicles (UAVs) are known for having a wide variety of applications ranging from landscape surveying, industrial inspection and monitoring to precision agriculture and aerial imaging. The extensive use of UAVs can be linked to the cost-effective solutions provided by them. Important advantages of multimotored vehicles compared to single rotor vehicles are the increased lifting capacity, smoother vertical flight and safety redundancy. Moreover, lower manufacturing and production values combined with the lack of a human pilot decrease acquisition and operating costs significantly. Thus, there is a large shift across the aviation industry to use UAVs instead of conventional manned aircrafts. On a general basis, UAVs are usually dimensioned and optimized for missions. This is where CFD can come in handy as it can predict the flow characteristics and help to further optimize the UAV for the mission it is designed for (Vijayaraghavan, 2019; Wilhelm, 2015; Winter, 2013).

Beside experimental measurements Computational Fluid Dynamics (CFD) simulations play an increasing role for analysis and design of such fluid flow problems. For instance, turbomachinery design has been strongly supported by CFD. First, CFD has been employed as flow analysis tool and over the last decades it has been more and more integrated in the design process of turbomachinery. The benefit ranges from shorter design cycles over cost reduction to performance optimization (Denton & Dawes, 1999).

Accurate prediction of rotorcraft performance continues to be challenging. The flows are inherently unsteady, nonlinear, and complex. For instance, a rotor blade can encounter its own tip vortex and the tip vortices of other blades.

It is even more difficult when there are aerodynamic interactions between multiple rotors and fuselage because of the proximity of all these components (Diaz & Yoon, 2018).

The scope of this study was to analyze and compare the effects of a toroidal propeller and a considered conventional geometry by simulating a free-standing propeller, the method used in this study is the MRF (Multi Reference Frame) method, and the results for velocity, mass flow flux were compared to determine if there is a significant interference of the toroidal propeller in the fluid flow.

2. NUMERICAL METHODOLOGY

For a fluid, there are a set of equations that govern the proprieties of a fluid, the Navier-Stokes, that describe continuity (1), momentum (2) and energy (3). In an incompressible flow, compressibility effects are considered and ρ constant, which means the mass conservation equation can be written as is in Eq (4). The change of volume in the fluid is inexistent, so the equation of conservation of momentum is reduced to the form described in Eq (5). The energy equation is not included as there is no coupling between the momentum and conservation of mass equations because of which the pressure field is not unique (Henningson & Berggren, 2005).

$$\frac{\partial p}{\partial t} + p\frac{\partial u_k}{\partial u_k} = 0 \tag{1}$$

$$\rho\frac{\partial u_i}{\partial t} = -\frac{\partial p}{\partial x_i} + \frac{\partial \tau_{ij}}{\partial x_j} + \rho F_i \tag{2}$$

$$\rho\frac{\partial e}{\partial t} = -\rho\frac{\partial u_i}{\partial x_i} + \Phi + \frac{\partial}{\partial u_i}\left(k\frac{\partial T}{\partial u_i}\right) \tag{3}$$

The geometries used in this study are shown in Figure 1 – a) for the toroidal propeller which dimensions are 80 mm of length and 40 mm of width, and in Figure 1 – b) for the conventional propeller with the measurements of 80 millimeters of length and the maximum width of 8 mm and minimum of 2 mm. The domain of the simulation is shown in Figure 2 which is a cylinder with 240 mm of width and 800 mm of length, for this numerical study, the propeller will be placed in the center of the geometry.

$$\frac{\partial u_i}{\partial x_i} = 0 \tag{4}$$

$$\frac{\partial u_i}{\partial t} + u_j\frac{\partial u_i}{\partial x_j} = -\frac{1}{\rho}\frac{\partial p}{\partial x_i} + \upsilon\nabla^2 u_i + F_i \tag{5}$$

Calculations were performed in the open-source software OpenFOAM. As can be seen by many studies from the literature, the MRF (Multi Reference Frame) mathematical approach for the motion of the propeller is best advised for accuracy and computational cost (OpenFOAM Foundation, 2022; Vijayaraghavan, 2019).

a) b)

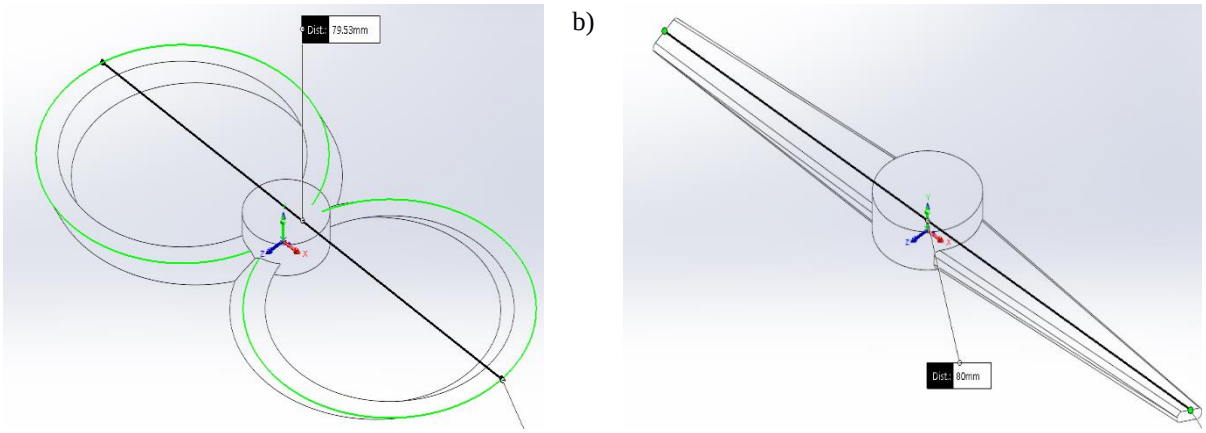

Figure 1 – a) CAD design of the toroidal propeller; b) CAD design of the conventional propeller.

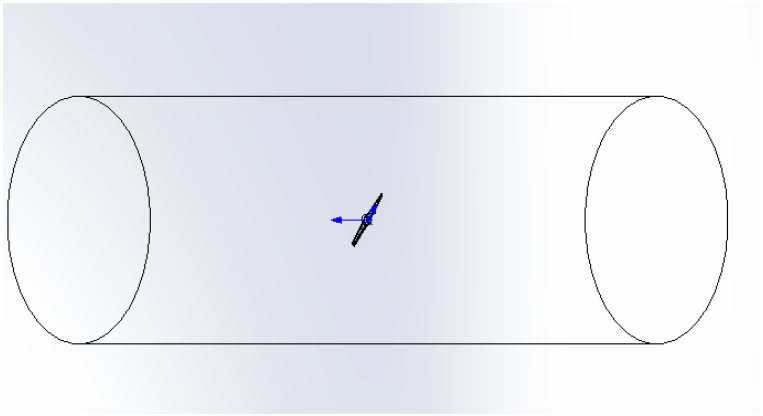

Figure 2 – CAD domain of the case.

This method computes fluid flow using the stationary and rotating reference frames, Figure 3 shows the level of refinement required in the propeller to achieve the proper solution of the MRF method. The governing equations of the method can be split into rotating and stationary part as described by Eq (6) and Eq (7).

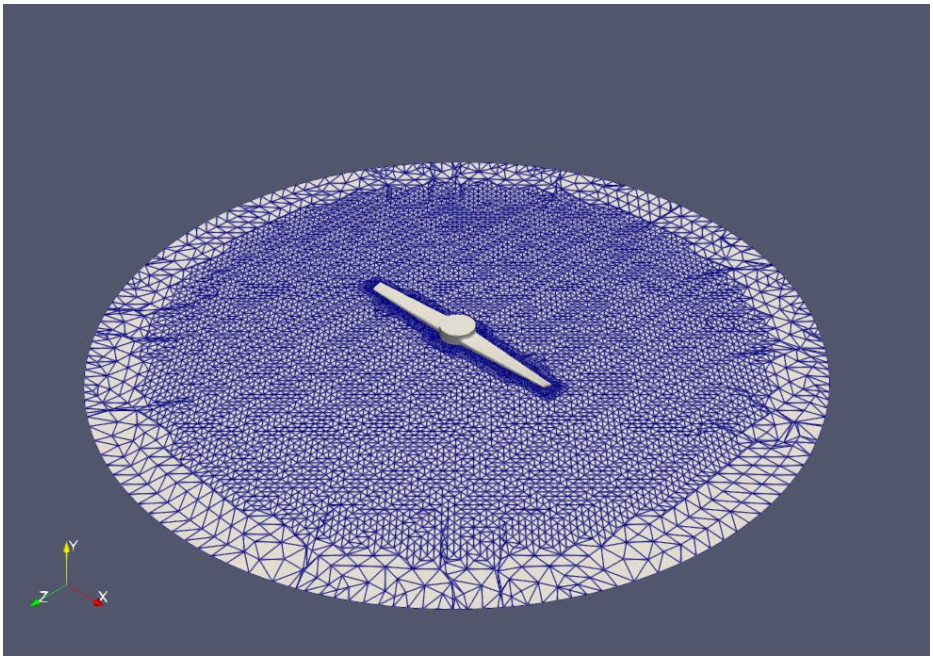

Figure 3 – Refinement level around the propeller.

Stationary part:

$$\nabla \cdot (u_1 u_i) = -\nabla_p + \nabla \cdot (u_{eff}(\nabla u_1 + (\nabla u_i)^T)) \quad (6)$$

$$\nabla \cdot u_1 = 0$$

Rotating part:

$$\nabla \cdot (u_R u_i) + \Omega \, x \, u_1 = -\nabla_p + \nabla \cdot (u_{eff}(\nabla u_1 + (\nabla u_i)^T)) \quad (7)$$

$$\nabla \cdot u_R = 0$$

For the calculation of the continuous phase, the RANS method and k – ε model is considered for mathematical closing as is shown in Eq. 8 (for k) and Eq. 9 (for ε) (Diaz & Yoon, 2018). The boundary conditions for the velocity and pressure of setup to the case are in **Erro! Fonte de referência não encontrada.**. Calculations were made with the time step for every iteration of 0.001 seconds and the velocity of the propeller is 1,200 revolutions per minute. The results obtained were used as a basis for the Grid Convergence Index (GCI) (*apud.* Sasse 2023) method, where the analysis variable was the point speed of different mesh refinements, with these data it was possible to determine the appropriate mesh with the lowest computational cost and reliability of results. The refinement level of each mesh is shown in Figure 4 for Meshes 1, 2 and 3 and the results for the GCI method are shown in Figure 5.

$$\frac{\partial}{\partial t}(f_k \rho_k k_k) + \nabla \cdot \left(f_k \left[\rho_k v_k k_k - \left(\mu_k + \frac{\mu_k^t}{\sigma_k} \right) \nabla k_k \right] \right) = f_k (P_k - \rho_k \varepsilon_k) + \sum_{k \neq j}^{n_f} T_{kj}^{(k)} \tag{8}$$

$$\frac{\partial}{\partial t}(f_k \rho_k \varepsilon_k) + \nabla \cdot \left(f_k \left[\rho_k v_k \varepsilon_k - \left(\mu_k + \frac{\mu_k^t}{\sigma_\varepsilon} \right) \nabla \varepsilon_k \right] \right) = f_k \frac{\varepsilon_k}{k_k} (C_1 P_k - C_2 \rho_k \varepsilon_k) + \sum_{k \neq j}^{n_f} T_{kj}^{(\varepsilon)} \tag{9}$$

Fields	Boundary Conditions
Inlet	fixedValue (0 -7.5 0)
Outlet	pressureInletOutletVelocity (0 0 0)
Wall	noSlip
Propeller	noSlip

Table 1 – Boundary conditions to setup the case.

a) c) e)

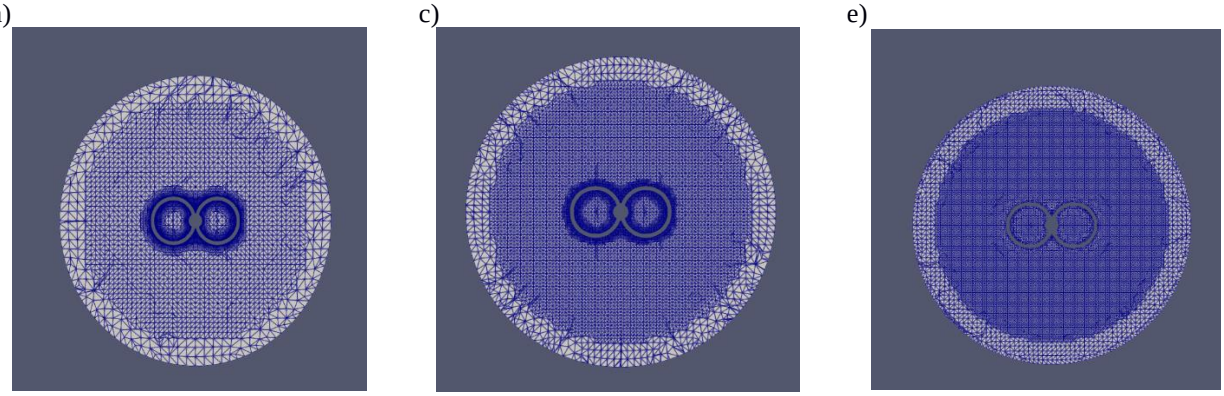

b) d) f)

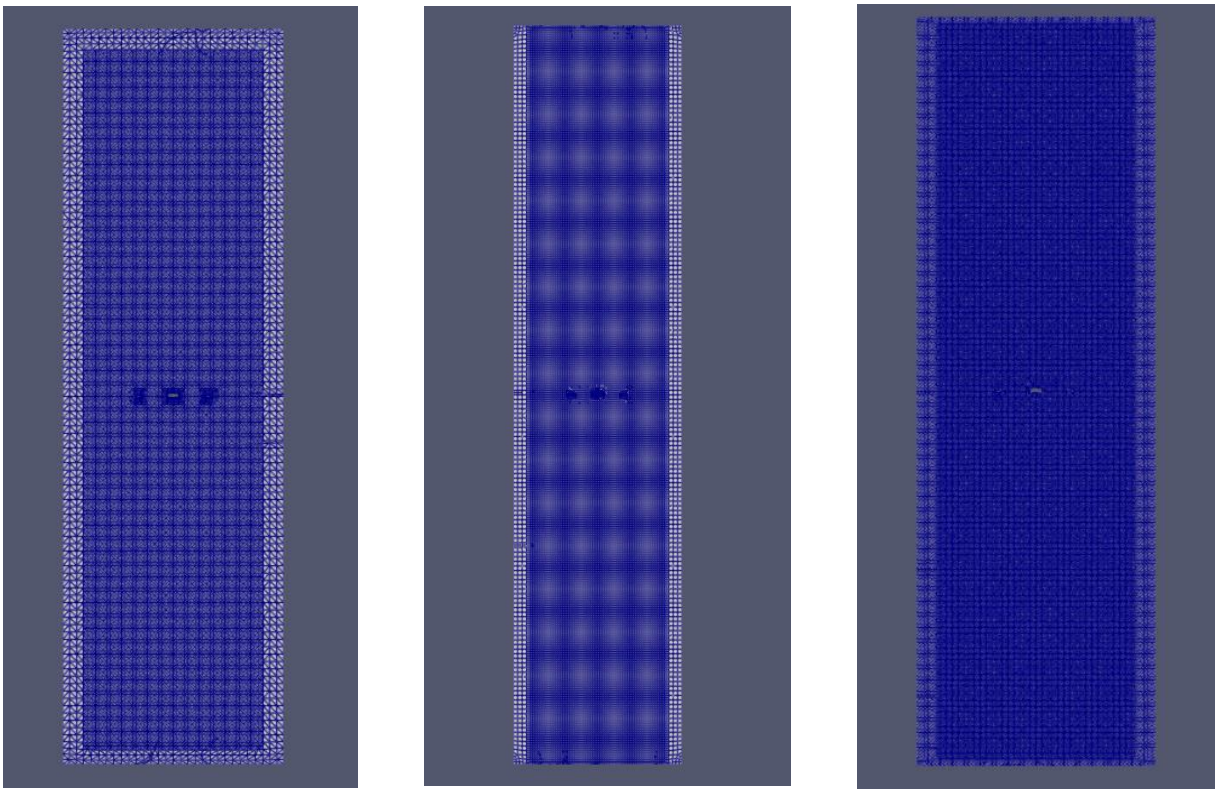

Figure 4 – a) Axial section of Mesh 3 with 667,134 cells; b) Longitudinal section of Mesh 3 with 667,134 cells; c) Axial section of Mesh 2 with 1,750,320 cells; d) Longitudinal section of Mesh 2 with 1,750,320 cells; e) Axial section of Mesh 1 with 3,303,649 cells; f) Longitudinal section of Mesh 1 with 3,303,649 cells.

Although the results do not present a concrete convergence in relation to the refinement of the numerical mesh, it was decided to use the intermediate mesh due to computational limitations, since the deviation in relation to the more refined mesh is relatively small. Therefore, it was decided to use the intermediate mesh, which contains 1,750,320 computational cells, in order to balance the reliability of the results and the lowest computational cost.

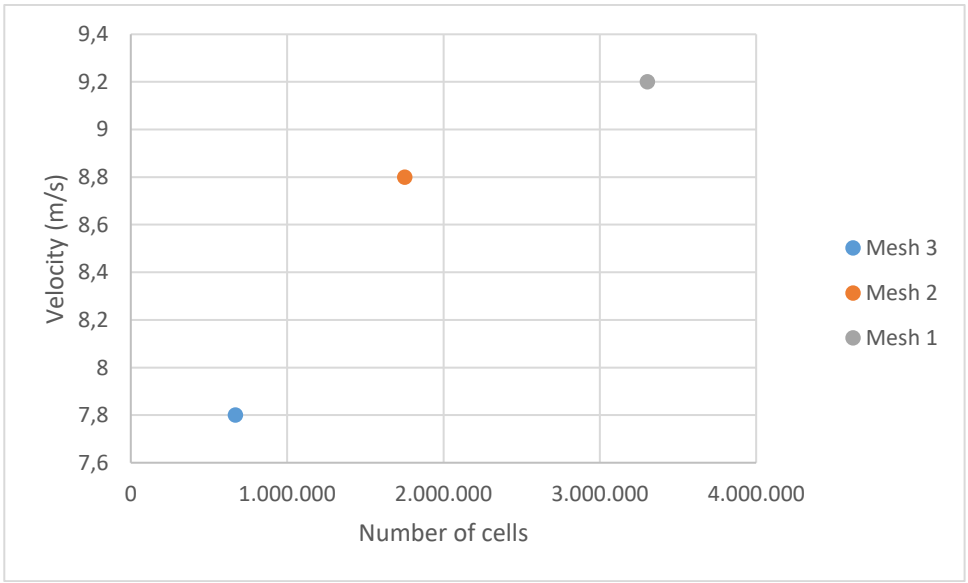

Figure 5 – Velocity with three refinement levels of the meshes

3. RESULTS

3.1 PARAMETRIC STUDY OF THE TOROIDAL PROPELLER

In the development of a toroidal thruster, it is critical to determine the tilt angle of its propeller to achieve the desired shape. This section addresses the parametric study performed on three rotors with inclination angles of 140°, 150° and 160°, under the same simulation conditions, as illustrated in Figure 6. The objective is to define the geometry that produces the highest flow velocity.

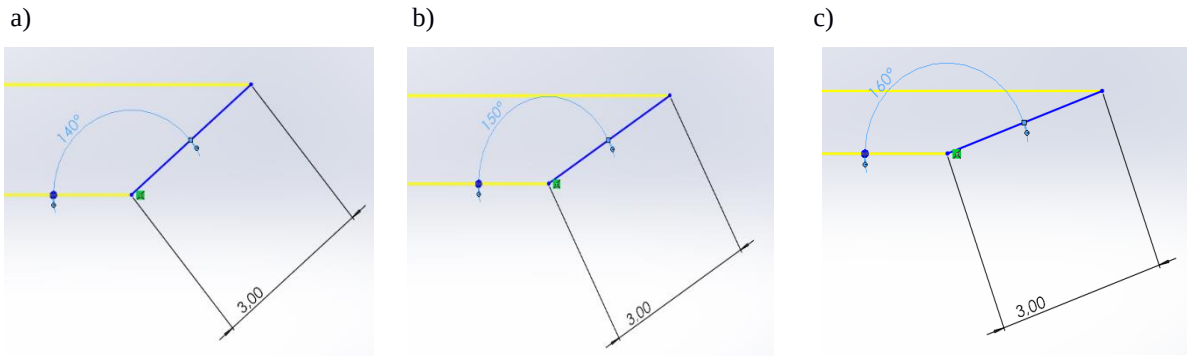

Figure 6 - CAD profile of toroidal propeller with 140◦ of inclination; b) CAD profile of toroidal propeller with 150° of inclination; c) CAD profile of toroidal propeller with 160° of inclination.

The comparison method consisted of defining a reference line in the axial direction of the flow domain to obtain the velocity profile of the three geometries. The velocity was defined by capturing data in two distinct regions located 20 mm above and below the rotor, considering the interference of the geometry in the flow. As shown in Figure 7 and Figure 8, the results indicate that the most efficient toroidal thruster has a 150° tilt angle. Based on these results, the same analysis criteria will be used to compare the most efficient propeller with a conventional one.

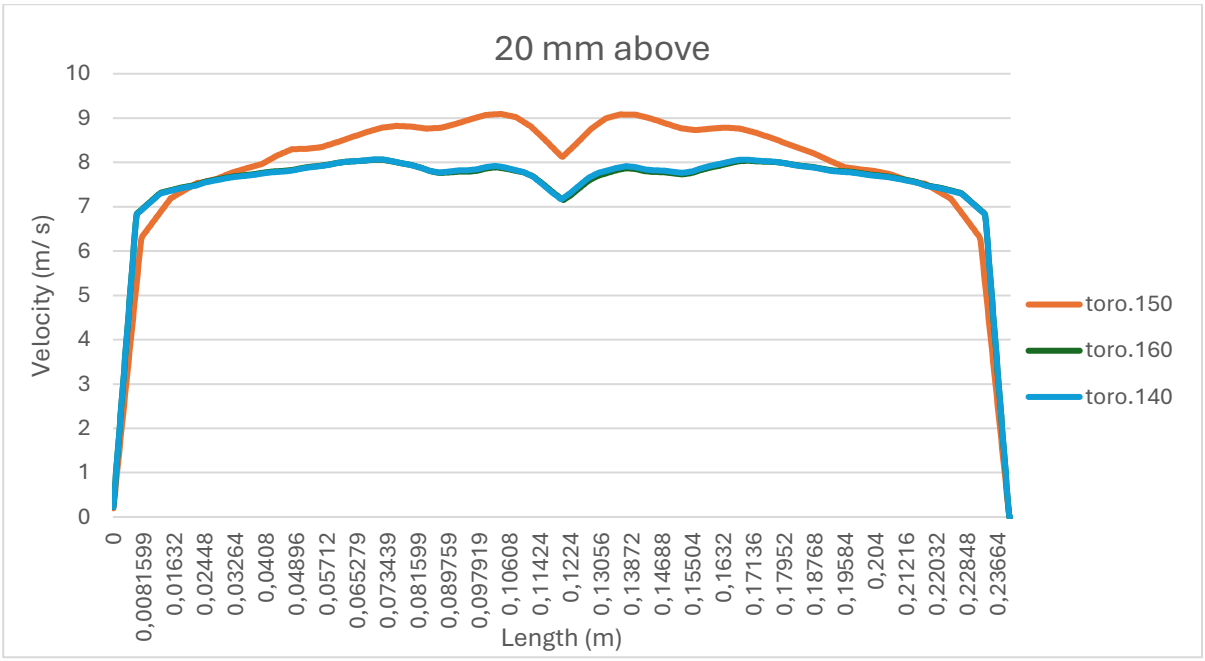

Figure 7- Velocity in the axial region 20 mm above the propeller

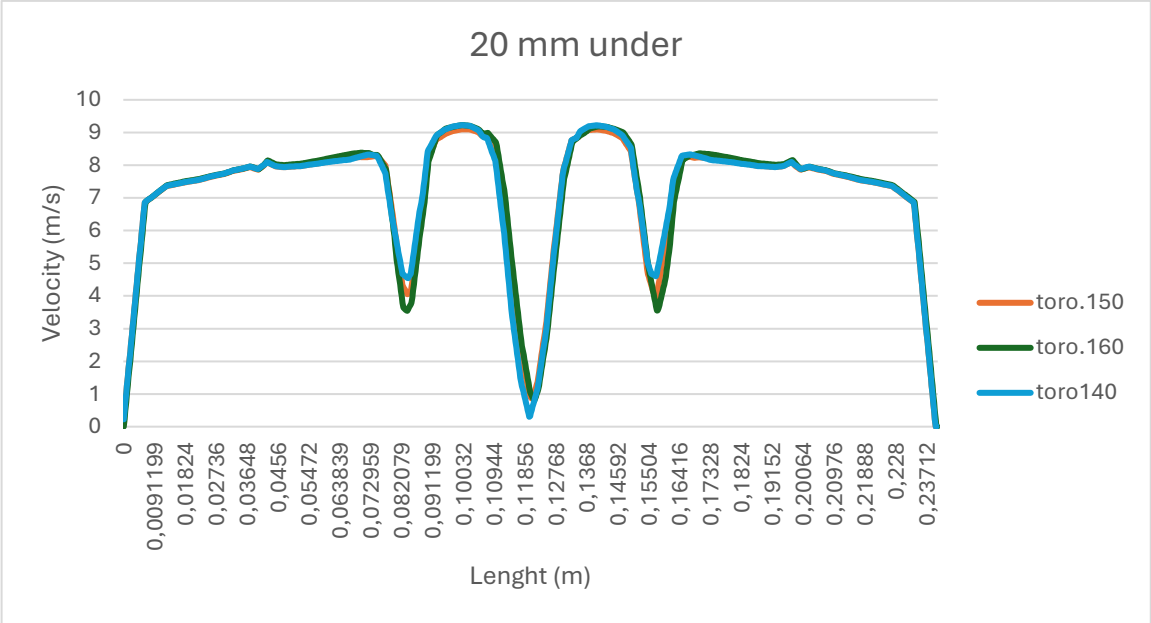

Figure 8- Figure in the axial region 20 mm under the propeller

3.2 COMPARISON BETWEEN TOROID AND CONVENTIONAL

By analyzing the same velocity profiles obtained through the geometries, and comparing them, it was possible to notice the increase in the flow velocity at 20 mm before the rotor, in the said suction zone, as shown in Figure 9, and an increase at 20 mm below the rotor, in the dispersion zone, as illustrated by Figure 10.

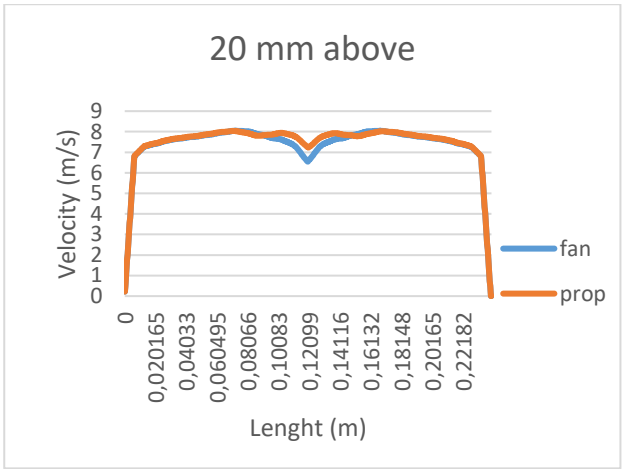

Figure 9- Velocity 20 mm above the propeller

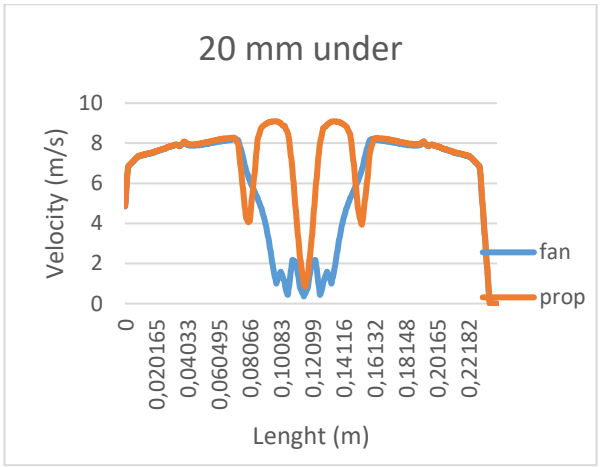

Figure 10- Velocity 20 mm under the propeller

From these data of the velocity profiles, it is possible to speculate about why the flow generated by the toroidal geometry rotor has this behavior, as illustrated in Figure 11, and why it is superior to the conventional one.

a) b)

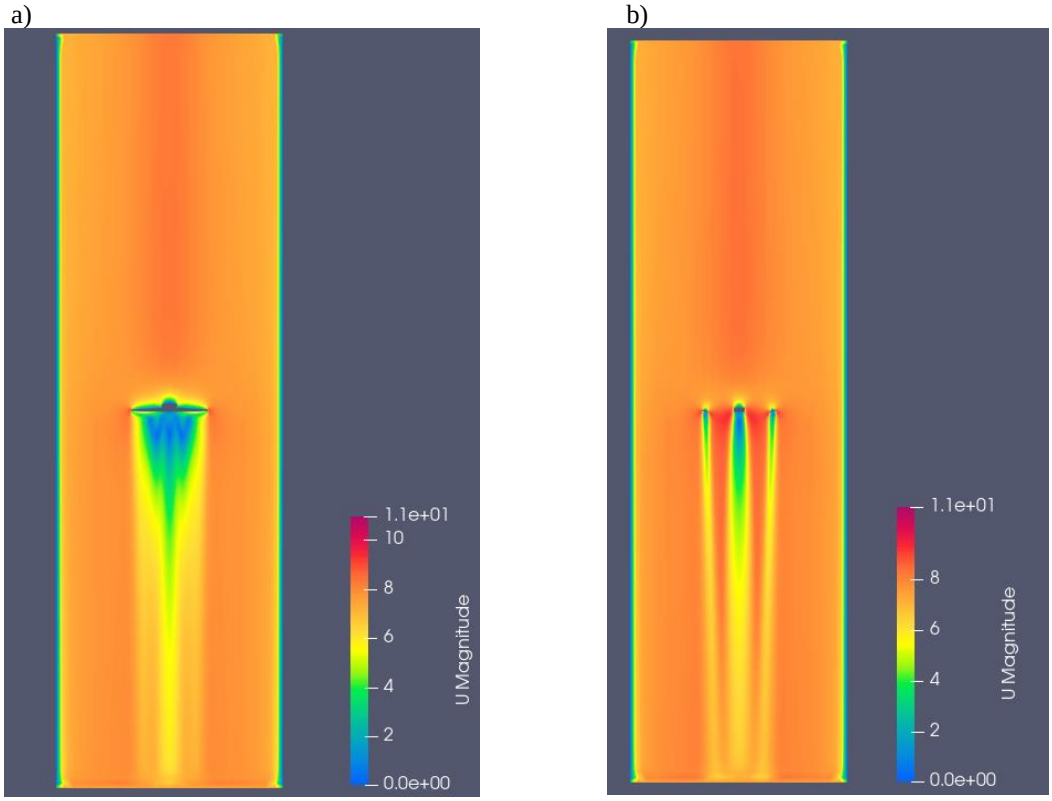

Figure 11- a) Velocity profile generated by the conventional propeller; b) Velocity profile generated by the toroidal propeller.

As the time to carry out this was short, it was not possible to observe the computational data with greater reflection, but it is possible to speculate that due to the toroidal shape of the thruster, it causes a smoother flow when it encounters the fluid, and thus allows an increase in the flow velocity. This would explain the behavior of the turbulent kinetic energy profile, where in toroidal geometry it is concentrated in a central section below the thruster, while in conventional geometry, it induces the kinetic energy to be more diffuse, as shown in Figure 12.

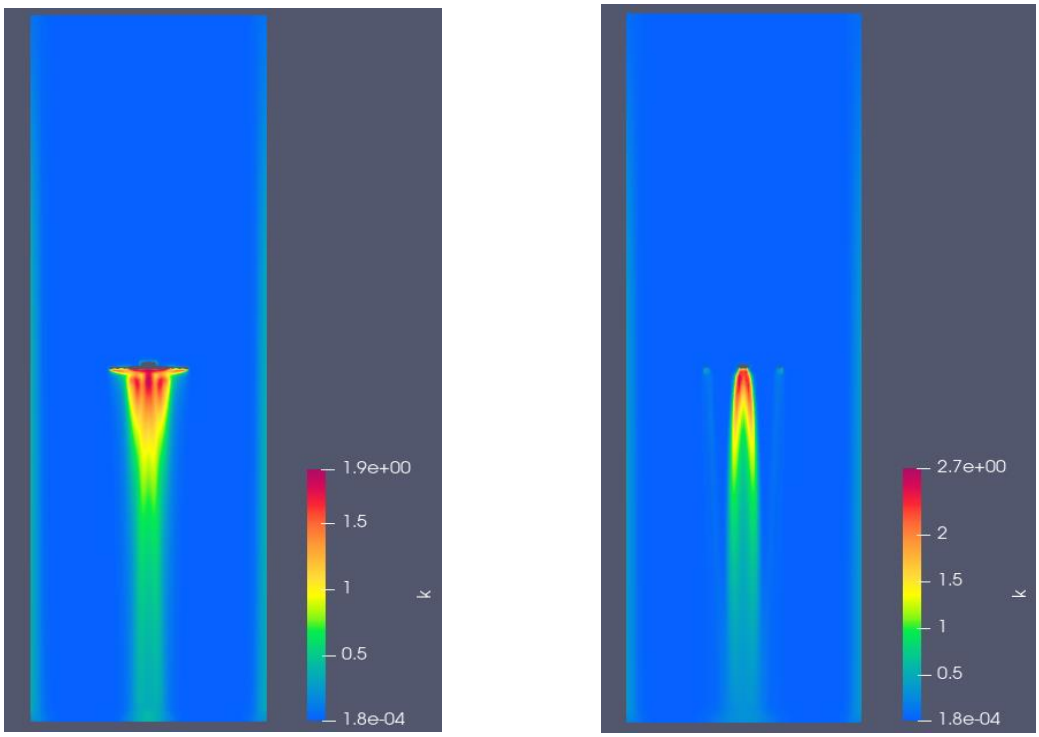

Figure 12- a) Turbulent view of the air flow generated by the conventional propeller; b) Turbulent view of the air flow generated by the toroidal propeller

4. CONCLUSIONS

The results presented in the previous section indicate that, by means of numerical analysis and considering the established conditions, the toroidal geometry thruster provides a higher flow velocity in both the suction and dispersion phases, compared to the conventional geometry. This is shown in Table 2, which presents data regarding the inlet pressure, the flow rate and the velocity in the flow contour determined as the outlet.

Geometry	**Velocity (m/s)**	**Pressure (Pa)**	**Flow Rate (m^3/s)**
Toroidal	7,8	2,1	4,5
Conventional	7,5	1,8	4,2

Table 2- Pressure, velocity and flow rate in the outlet of the domain

Based on these results, it can be preliminarily inferred that the toroidal geometry presents a differential in the formation of the flow profile, due to its larger contact area with the fluid. This geometric configuration, with its smooth, rounded surface, facilitates fluid movement in a way that minimizes significant losses in the velocity profile.

5. REFERENCES

Denton, J. D., & Dawes, W. N. (1999). Computational fluid dynamics for turbomachinery design. *Proceedings of the Institution of Mechanical Engineers, Part C: Journal of Mechanical Engineering*, *213*(2), 107–124. https://doi.org/10.1243/0954406991522211

Diaz, P., & Yoon, S. (2018). High-Fidelity Computational Aerodynamics of Multi-Rotor Unmanned Aerial Vehicles. *AIAA SciTech Forum*, 1–22.

Henningson, D. S., & Berggren, M. (2005). *Fluid Dynamics: Theory and Computation*.

OpenFOAM Foundation. (2022). *OpenFOAM the Open Source CFD Toolbox User Guide*.

Vijayaraghavan, S. (2019). *Simulation of rotating elements of a quadcopter using OpenFOAM*.

Wilhelm, D. (2015). Rotating Flow Simulations with OpenFOAM. *International Journal of Aeronautical Science & Aerospace Research (IJASAR), S1:001*, 1–7. http://scidoc.org/IJASAR.php

Winter, M. (2013). *Benchmark and validation of Open Source CFD codes, with focus on compressible and rotating capabilities, for integration on the SimScale platform*.

6. RESPONSIBILITY NOTICE

The authors are responsible for the printed material included in this paper